

Article

A Comparison of Lithium-Ion Cell Performance across Three Different Cell Formats

Grace Bridgewater ¹, Matthew J. Capener ¹, James Brandon ¹, Michael J. Lain ^{1,*}, Mark Copley ¹ and Emma Kendrick ^{1,2} 

¹ Warwick Manufacturing Group, University of Warwick, Coventry CV4 7AL, UK; g.bridgewater.1@warwick.ac.uk (G.B.); m.capener@warwick.ac.uk (M.J.C.); wmg@warwick.ac.uk (J.B.); mark.copley@warwick.ac.uk (M.C.); e.kendrick@bham.ac.uk (E.K.)

² School of Metallurgy and Materials, University of Birmingham, Birmingham B15 2TT, UK

* Correspondence: m.j.lain@warwick.ac.uk

Abstract: To investigate the influence of cell formats during a cell development programme, lithium-ion cells have been prepared in three different formats. Coin cells, single layer pouch cells, and stacked pouch cells gave a range of scales of almost three orders of magnitude. The cells used the same electrode coatings, electrolyte and separator. The performance of the different formats was compared in long term cycling tests and in measurements of resistance and discharge capacities at different rates. Some test results were common to all three formats. However, the stacked pouch cells had higher discharge capacities at higher rates. During cycling tests, there were indications of differences in the predominant degradation mechanism between the stacked cells and the other two cell formats. The stacked cells showed faster resistance increases, whereas the coin cells showed faster capacity loss. The difference in degradation mechanism can be linked to the different thermal and mechanical environments in the three cell formats. The correlation in the electrochemical performance between coin cells, single layer pouch cells, and stacked pouch cells shows that developments within a single cell format are likely to lead to improvements across all cell formats.

Keywords: lithium-ion; cell formats; coin cells; pouch cells



Citation: Bridgewater, G.; Capener, M.J.; Brandon, J.; Lain, M.J.; Copley, M.; Kendrick, E. A Comparison of Lithium-Ion Cell Performance across Three Different Cell Formats. *Batteries* **2021**, *7*, 38. <https://doi.org/10.3390/batteries7020038>

Academic Editor: Mohammad (Mim) Rahimi

Received: 18 March 2021

Accepted: 8 May 2021

Published: 8 June 2021

Publisher's Note: MDPI stays neutral with regard to jurisdictional claims in published maps and institutional affiliations.



Copyright: © 2021 by the authors. Licensee MDPI, Basel, Switzerland. This article is an open access article distributed under the terms and conditions of the Creative Commons Attribution (CC BY) license (<https://creativecommons.org/licenses/by/4.0/>).

1. Introduction

When developing a lithium-ion cell chemistry, it is necessary to produce prototypes in a fully sized cell format, to provide information on electrochemical performance, energy density, and safety. Before that, the cell chemistry is first optimised in a smaller format test cell, typically coin cells or an equivalent. The cell technology is then scaled up to a fully engineered stacked or wound prototype [1]. This approach is adopted by every lithium-ion cell manufacturer. New active materials, electrolytes or electrode formulations are evaluated on a small scale, and then progressively scaled up to full sized cells. This can be in a cylindrical, prismatic or soft pouch enclosure [1], depending on the target application and previous capital investment in specific cell making equipment.

There is always a dilemma about when to transition from a test cell format to a fully engineered cell. Generally, confidence in performance extrapolation from coin cells to prototype cells is low. A key benefit of coin cells is that large numbers of cells can be produced from a single mix, requiring only a few grams of active material. Coin cells provide a very useful comparison, but they have limitations, because of their design and construction. They use a significant excess of electrolyte, and the cell body has a relatively large thermal mass. Both of these can mask problems that will only become evident in a full-sized cell. Additionally, realistic values of energy density and power density can only be measured in a properly engineered stacked or wound cell, though values can be estimated using various modelling approaches, based on coin cell data. Generally, models are good at predicting energy density. Power density can be more difficult to calculate,

because of the various different contributions to the overall cell resistance. Manufacturing full size cells requires more materials, to produce double sided coatings, and the various cell making steps also involve much more time and effort. Clearly, it would be useful to be able to predict accurately the performance properties of a stack or wound cell format from a smaller cell format.

In this work, we are developing lithium-ion cells for high power applications like hybrid electric vehicles (HEV). Typically, electrodes for this type of cell have low areal capacities, thicker metal foils, relatively high porosities, and a greater amount of conductive carbon in the electrode formulation [2]. During cell development, it is useful to know whether the performance measured in coin cells is representative of full-sized cells. Therefore, cells have been made in three cell formats, using the same electrode coatings. This avoided the scale up issues that are associated with mixing and coating [3]. The cell types are coin cells, stacked pouch cells, and as an intermediate, pouch cells with two single sided electrode pieces. Various properties of these cells are compared in Table 1.

Table 1. Comparison of different cell formats.

Property		Coin Cell	Single Sided Pair	Stacked Pouch
Active material in mix	/g	10	100	1000
Anode area	/cm ²	1.77	35.0	1330
Cathode area	/cm ²	1.72	33.2	1196
Cell making		Manual	Manual	Semi-automated
Half-cell option		Routine	Possible	Difficult
Reference option		Alternatives	Possible	Possible
Cell	/g	4.4	19.0	35.0
Electrolyte	/g	0.06	1.0	9.0

Performance properties have been studied in cells across different cell formats with a range of scales, as illustrated in Table 2 [4–9]. Similar cycling performance was achieved across three widely ranging cell sizes [4]. Coin cells were used for accelerated cycle life tests, while pouch cells were used for expansion tests [5]. The performance of LFP cathodes patterned using very fast laser pulses was similar in Swagelok® (Solon, OH, USA) and pouch cells [6]; the pouch cell dimensions were specified in a parallel publication [10]. In a typical scale up project, coin cells were used to identify promising electrode compositions, and establish optimum cycling protocols [7]. These were then applied to pouch cells, which were subjected to a range of tests including rate tests, hybrid pulse power characterisation (HPPC) [11], and cycling tests. By way of contrast, the specification for a full-sized cell with a high energy density was used to work backwards to a coin cell specification [8]. This required lithium foil (<50 µm, not 250 µm), a high areal capacity (>3.5 mA h cm⁻²) and a low quantity of electrolyte (<3 g (A h)⁻¹). It is much easier to achieve long cycle life in a coin cell using thick lithium metal foils, low coat weight cathodes, and a significant excess of electrolyte. It can be difficult to make direct like for like comparisons of electrolyte quantity across cell formats because there is much more void space or dead volume (proportionately) in a coin cell than a stacked pouch cell [12,13].

In development work on lithium/sulphur cells, different degradation mechanisms were identified in the different cell formats [9]. In coin cells, the lithium polysulphide shuttle mechanism was the main issue. However, in pouch cells, the lithium metal was a greater problem, with the formation of dendrites, and ultimately powdering of the electrode material.

There are also cell format studies over a much narrower range of scales. For example, graphite + 8 wt% nano-silicon anodes and NMC-811 cathodes were used to make 0.75 A h pouch cells and 2.0 A h 18650 cylindrical cells [14]. The pouch cells were tested under various fixed or flexible pressures, to study the impact on the expansion and contraction of the silicon. The cylindrical cells confirmed the problems of inhomogeneous compression. After testing, electrodes from the pouch cells were extracted, and used to make coin cells

and symmetric pouch cells for further characterisation. There are several other examples where coin cells have been built using electrodes harvested from full sized cells [15–20]. This enabled cell level degradation processes to be attributed to one (or both) electrodes.

Table 2. Previous scale up tests using different cell formats.

Anode	Cathode	Coin Cell /mA h	Pouch Cell /A h	Scale Up Factor	Reference
Graphite	LiMn ₂ O ₄	5	1.5, 112	22,400	[4]
Graphite or Li ₄ Ti ₅ O ₁₂	LiCoO ₂ , LiMn ₂ O ₄ or doped LiMn ₂ O ₄	~2	50	25,000	[5]
Lithium or Graphite	Patterned LFP	1–2	0.022–0.044	22	[6]
Graphite	HE-NMC	~3	~0.4	133	[7]
Lithium metal	NMC-622	~5	1.0	200	[8]
Lithium metal	Sulphur	~20	1.5	750	[9]

Various cylindrical cells from 1.5 A h 18650 to 5.0 A h 21700 cells have been compared in two studies [21,22]. The energy density depended on the areal capacities of the electrodes but not the cell size. However, using a larger cell size, with a higher capacity, will reduce cell and module manufacturing costs, for the same battery energy. There are various modelling papers that compare properties across the three main formats [23,24]. The influence of thermal effects on cycling performance was modelled using a multi-scale, multi-domain framework [23]. Cell degradation was linked to the average cell temperature, and to non-uniformities in temperature and state of charge across the cells. The outcome of external short circuit tests was modelled using a multi-dimensional modelling approach, with a 2D electrical model and a 3D thermal model [24]. Cells with a high surface area to volume ratio were most likely to avoid thermal runaway.

Even for relatively simple coin cells, care is required to achieve consistent and useful results. In particular, cell assembly must use a repeatable methodology [25], and cell testing results need to be averaged over multiple, equivalent cells [26]. Even with this approach, x-ray spatial profiling revealed differences in compression across the electrode surface, and variable porosity in the polymeric separator [27]. Greater consistency was obtained for the alternative EL-CELL configuration using automated electrode handling and alignment during cell assembly [28].

2. Results

After cell formation is complete, the most common test applied to lithium-ion cells is long term cycling. However, there are a wide range of other tests that give useful and complementary information. The effect of discharge rate on discharge capacity is important in many applications. In this study, the rate tests were performed in separate tests, rather than combined with cycling tests. HEV drive cycles involve short charge and discharge pulses, which is a different test from full, continuous discharge, following a low-rate charge. Therefore, short duration charge and discharge pulse tests were performed, at rates up to 50 C. A useful measurement of cell resistance is area specific impedance (ASI). This is also measured with a sequence of short pulses [29]. The galvanostatic intermittent titration technique (GITT) is an intermediate between the short ASI pulses and full discharge. The voltage transients during a series of fixed current pulses are analysed, to interpret the limiting mechanisms within the cell [30,31]. The GITT current density and step durations should be optimised for different cell chemistries [32].

Batches of ten cells were prepared for each of the three cell formats, based on a cathode capacity of 1 mA h cm⁻² and an excess anode capacity of 10%. In the Supplementary Materials, properties are calculated for the three cell formats and two different areal capacities. The lower areal capacity is typical for a cell optimised for high power applications, and the higher value for a cell designed for maximum energy density. During the cell assembly

processes, the weights of all the components were measured and recorded. As a comparison, Figure 1a shows the calculated coat weights of the NMC-622 active material in the cathode ($\text{gsm} = \text{g m}^{-2}$). The stacked pouch cells values are the same because an average weight per electrode was used. The larger variation for the coin cells reflects the much smaller electrode area, and fluctuations in coat weight along and across the coating. Coat weight measurements recorded using the Mesys system gave a $\pm 2\%$ variation for the anode coating and $\pm 4\%$ for the cathode coating. This compared to $\pm 1\%$ and $\pm 3\%$, respectively, for 3 mA h cm^{-2} coatings, which were prepared for a parallel project. The systematic trend for the coin cells was due to matching of anode and cathode weights, to maintain a consistent anode: cathode capacity ratio. These coat weights and other measurements from the formation cycle are summarised in Table 3. The values in brackets are standard deviations. The areal discharge capacities are plotted in Figure 1b.

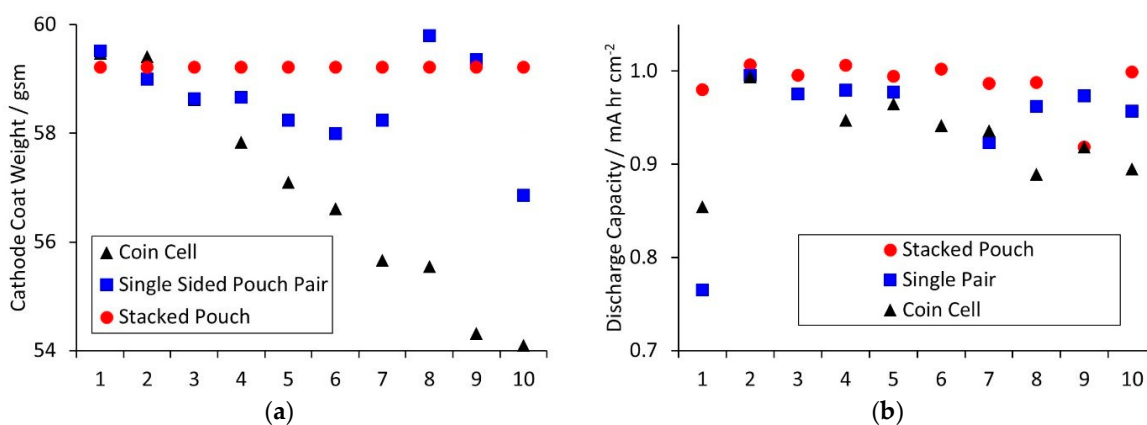


Figure 1. Cell properties with (a) cathode coat weights calculated from cell build data and (b) areal discharge capacities measured during formation.

Table 3. Formation cycle measurements for different cell formats.

Measurement		Coin Cells	Single Pouch Pair	Stacked Pouch
Coat Weight	/gsm	56.3 (1.7)	58.6 (0.8)	59.2 (N/A)
Discharge capacity	/mA h cm ⁻²	0.936 (0.033)	0.985 (0.020)	0.988 (0.024)
Discharge energy	/mW hr cm ⁻²	3.49 (0.13)	3.63 (0.08)	3.65 (0.09)
First cycle loss	%	15.7 (0.8)	15.3 (1.3)	17.4 (1.8)
Average discharge voltage	/V	3.728 (0.019)	3.680 (0.007)	3.691 (0.001)

The cell voltages recorded during the tests, the actual first cycle loss (FCL) values, and the areal discharge energies are plotted in the Supplementary Materials. Coin cell 3 and single sided pouch pair cell 6 were defective, and coin cell 1 and single sided pouch pair 1 had low discharge capacities. All four of these cells were excluded from the mean and standard deviation calculations. The lower mean areal capacities for the coin cells reflected the spread of coat weights. The first cycle loss was due to the formation of solid electrolyte interphase (SEI) layer on the surface of the anode particles. The higher FCL for the stacked pouch cells was due to the anode coatings on the outside of the two end pieces in the stack. The average discharge voltage values were obtained by dividing the discharge energy (W hr) by the discharge capacity (A h) [33]. This value depends mainly on the cell chemistry but also has some contribution from the cell internal resistance.

To characterise the cycle life, two test protocols were applied to all three cell types, cycling at $\pm C/2$ and $\pm 3 C$. The former is a typical regime for all lithium-ion cells, whereas the latter is more applicable for cells intended for high-rate applications, and also accelerates the degradation processes within the cell. The discharge capacities for the two tests are shown in Figure 2. Coulombic efficiencies for the tests are given in the Supplementary Materials. For cycling at $\pm C/2$, the cycles to 80% of initial capacity were 225

and 300 (coin cells), 300 and >500 (single sided pouch cells), and >500 (stacked pouch cells). Linear extrapolation predicted around 1000 cycles to 80% for the stacked pouch cells. The cycle life was better than the coulombic efficiency would suggest. To achieve five hundred cycles above 80% of initial capacity, the average efficiency needs to be above 99.955% ($0.99955^{500} = 0.798$). The observed cycle life therefore implies some reversible self-discharge or side reactions that do not consume active lithium [34]. For cycling at ± 3 C, the cycles to 80% of initial capacity were 1000 (coin cell), 1300 and 1400 (single sided pouch cells), and 1550–1675 (stacked pouch cells). Thus, for both tests, capacity retention was clearly best in the stacked pouch cells. One single sided pair cell on each test almost matched the stacks, but the other was closer to the coin cells.

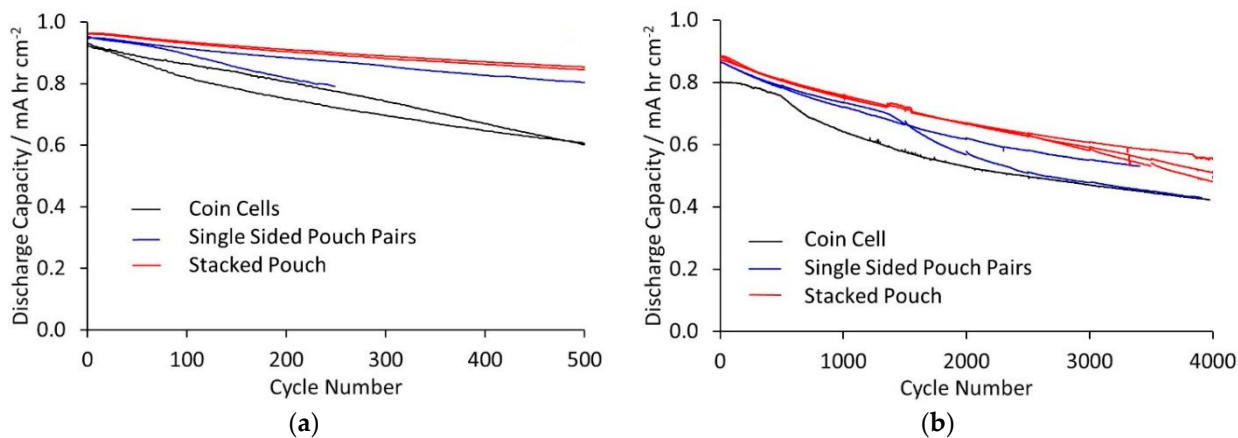


Figure 2. Discharge capacities during cycling at (a) $\pm \text{C}/2$ and (b) ± 3 C.

The ± 3 C cycle protocol included a cell characterisation test every five hundred cycles; the detailed steps are described in the Materials and Methods section (Section 4). Figure 3 shows the 5 C pulses for one of the stacked cells, and the calculated DC resistances for all of the cells. Examples of the 5 C pulses for the other cell types are contained in the Supplementary Information, along with comparisons before cycling and after one thousand cycles. There was a clear difference between the stacked pouch cells and the other two cell types. For the stacked pouch cells, there was a steady increase in resistance with cycling, along with a slow decline in capacity. For the other cells, there was less increase in resistance up to one thousand cycles. However, beyond this point, the declining capacity meant that the cells were below 3 V after the 60% discharge, making the resistance values unrepresentative.

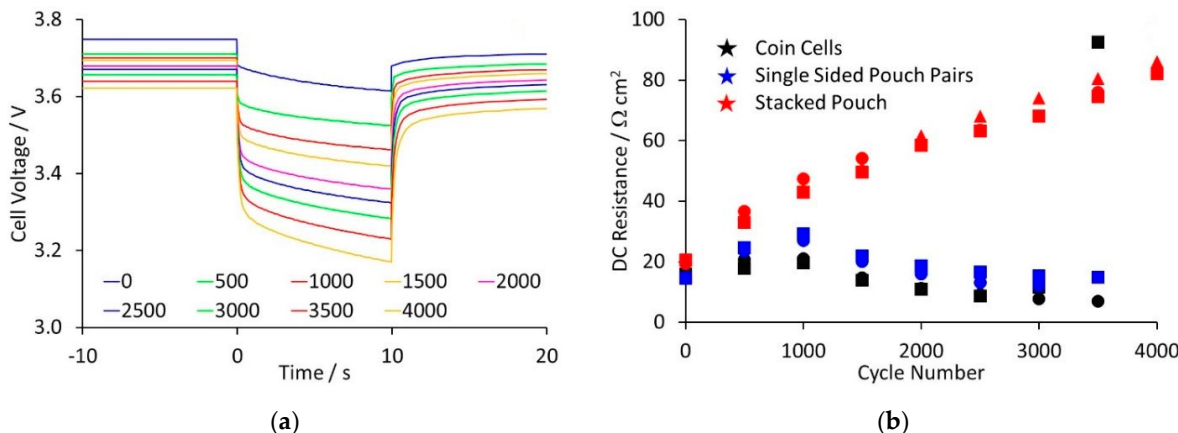


Figure 3. Periodic measurements during cycling at ± 3 C with (a) 5 C pulses for a stacked pouch cell and (b) calculated DC resistances.

During cycling, most cells show a loss of active lithium and an increase in their internal resistance. One analytical technique is to calculate the average voltages during charge and discharge [33]. Loss of active lithium shifts the relative state of charge of the two electrodes and increases the average voltages. An increase in resistance increases the difference between the average charge and discharge voltages. Results for the cells cycled on the $\pm C/2$ protocol are plotted in the Supplementary Materials. As with the cycling at ± 3 C, the coin cells showed predominantly loss of active lithium, and the stacked pouch cells mainly an increase in resistance.

The cells were intended for a high power application and were therefore subjected to resistance and rate performance tests. Area specific impedance (ASI) measurements were made on four-coin cells and four single sided pouch pair cells. The test protocol was based on the Argonne National Laboratory (ANL) methodology [29] and the requirements of the BatPac model [35]. To look at the relative contributions of the anode and cathode, equivalent measurements were also made on anode and cathode coin cell half cells. Plots of the cell voltages during the tests and the calculated ASI values are included in the Supplementary Materials. Average values for each cell are shown in Figure 4. One of the four coin cells was more resistive than the other three. Overall, the coin cells had slightly higher ASI values than the single pair pouch cells. Both were similar to the initial DC resistances in the ± 3 C cycling tests. The ASI values obtained for the coin cell half cells were interesting. As shown in the Supplementary Materials, there was a large increase in the cathode half cell ASI at low states of charge, so the increase seen in full cell ASI values at low states of charge was clearly due to the cathode. However, the theory underlying the ASI measurement technique predicts that $ASI_{total} = ASI_{anode} + ASI_{cathode} + ASI_{fixed}$ [36]. Therefore, the indication is that the lithium metal counter electrode makes a significant contribution to the ASI values in half cells.

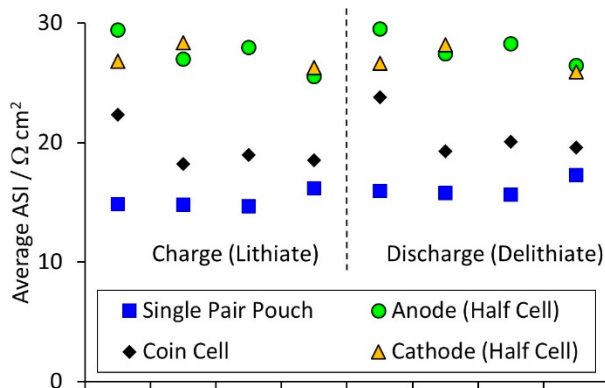


Figure 4. Averaged ASI measurements.

The voltage transients arising from constant current pulses can be analysed in three parts; an immediate IR change, ΔE_t , the voltage change during the transient, and ΔE_s , the change in rest voltage due to the change in state of charge [30]. Ten second pulses for the four cell types at 50% state of charge are presented in the Supplementary Materials. The main difference between the full cells and the half cells was in the IR drop, rather than ΔE_t or ΔE_s . The median values for IR were 15 and 30 mV for full cells and half cells on the initial pulse after a one-hour rest, and 10 and 20 mV for the subsequent reverse pulse. The ASI calculation is based on $IR + \Delta E_t - \Delta E_s$, so an increase in IR means an increase in ASI.

To investigate the ASI contribution from the lithium metal counter electrode, measurements were made in a symmetrical lithium // lithium cell. The combined ASI was around $8 \Omega \text{ cm}^2$, and the voltage change was almost all IR drop, with $\Delta E_t \sim 0$. This suggests the presence of an SEI film on the lithium metal surface. Before the pulse tests, the symmetrical cell went through one conditioning cycle, lasting one day. The half cells experienced multiple cycles, over several days. Therefore, the SEI layer on the lithium counter electrode

in the half cells was probably thicker, with a higher resistance. In consequence, the ASI values measured in the half cells were higher than in the full cells.

Another standard cell characterisation test is the discharge capacity as a function of the discharge rate. This test was applied to stacked pouch cells, single sided pouch pair cells, and anode and cathode coin cell half cells. Plots of cell voltage against capacity for representative cells are included in the Supplementary Materials. Plots of discharge capacity against discharge rate are shown in Figure 5; by analogy with Ragone plots [37], these are usually plotted as log–log graphs. The maximum rate that could be used with stacked cells was 30 C, due to the current limit of the test rig. Even so, at 30 C, the stacked cells clearly outperformed the single pair pouch cells.

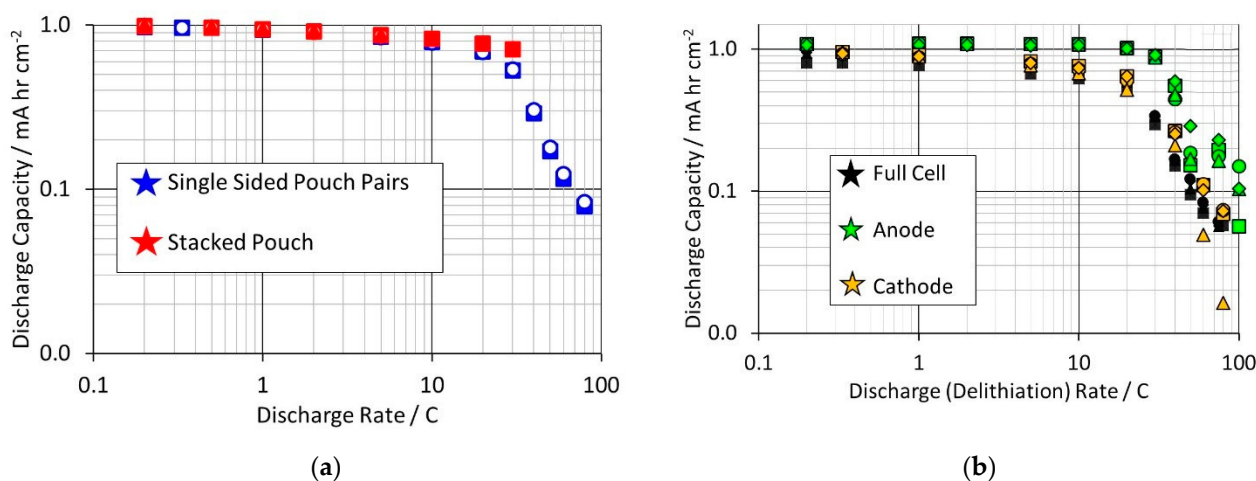


Figure 5. Discharge capacities at different rates for (a) single sided pair pouch and stacked pouch cells, and (b) coin cells.

The anode half cell tests were complicated by the creation of internal short circuits; in many cases the delithiation capacity was much higher than the lithiation capacity. High rate delithiation at the anode requires high-rate lithium deposition on the lithium metal, i.e., an increased risk of dendrite formation. The capacities were derived from the first maximum in the cell voltage, rather than waiting to reach the 1.5 V limit. Despite this, the anode capacities exceeded the cathode capacities, at the same rate. The full cells are clearly rate limited by the cathode rather than the anode.

Rather than high rate full, continuous discharge, many high-power applications involve relatively short charge and discharge pulses. Therefore, stacked pouch cells and single sided pair cells were subjected to sequences of two second and then ten second pulses. Examples of the voltage transients for each type are plotted in the Supplementary Materials. The stack cells were limited to 33 C by the maximum current capability of the equipment, but the single sided pairs were tested up to 50 C. The results are summarised in Figure 6, which shows the voltage transients at \pm C and \pm 20 C, for the ten second pulses. The ■ and ● symbols represent two, nominally equivalent cells. The transients showed two limiting processes. There was an immediate step change in voltage, followed by a linear change of voltage with time^{0.5}. Calculated values for the initial voltage drop and subsequent gradient are shown in Figure 7.

The initial voltage change was the difference between the voltages at time $t = 0$ for the 1 and 20 C pulses. This step change was due to the total cell resistance, including the tab resistance. The single sided pair and stacked pouch cells contained the same tabs, but the former have much lower capacity. This reduced the IR drop across the tabs, for the same rate, giving a smaller voltage change.

Galvanostatic intermittent titration technique or GITT tests are often performed on cells, as part of characterisation tests. For example, measurements of diffusion coefficient and open circuit voltage as a function of state of charge are very useful in cell modelling [20]. Therefore, a GITT discharge test was performed on one cell of each type, with

twenty-five C rate discharge steps of 150 s, alternating with one hour rest steps. Sets of transients are plotted in the Supplementary Materials. Figure 8 compares the $dV/dt^{0.5}$ gradients, and the open circuit voltages, for the three cells. There was good agreement across the cell types, except at low states of charge. The $dV/dt^{0.5}$ gradient, open circuit voltage and cell resistance all change rapidly with SoC in this range, at it is likely that there were small differences in the actual state of charge across the three cell formats.

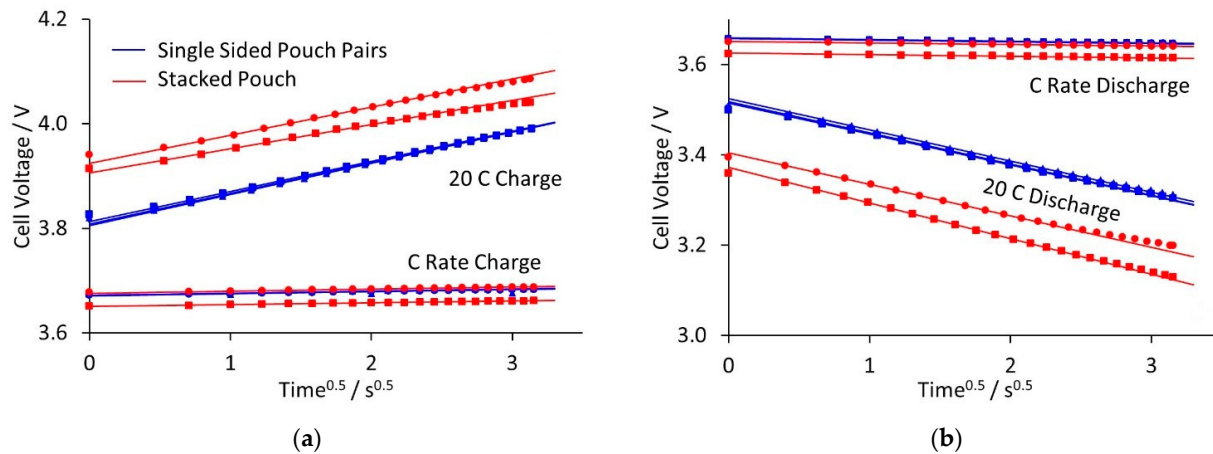


Figure 6. Cell voltages during ten second pulses for (a) charge and (b) discharge.

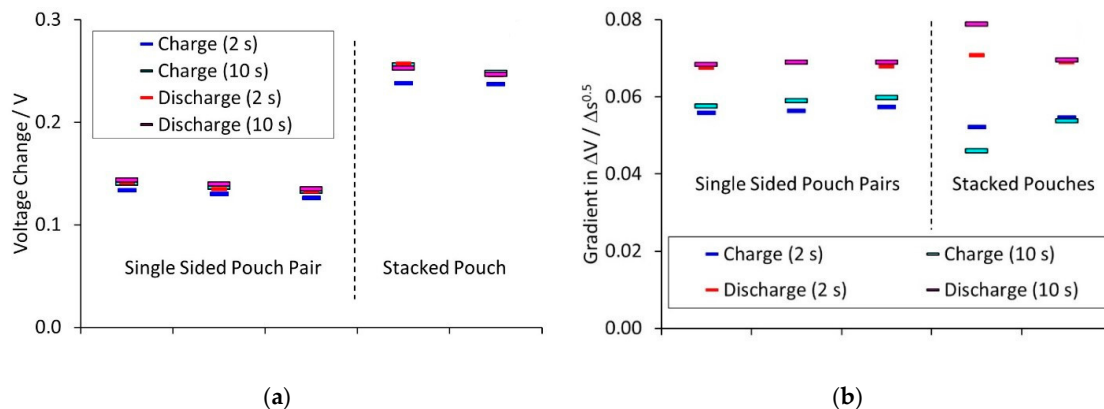


Figure 7. Analysis of 20 C charge and discharge pulses with (a) initial voltage drop and (b) gradient during transit.

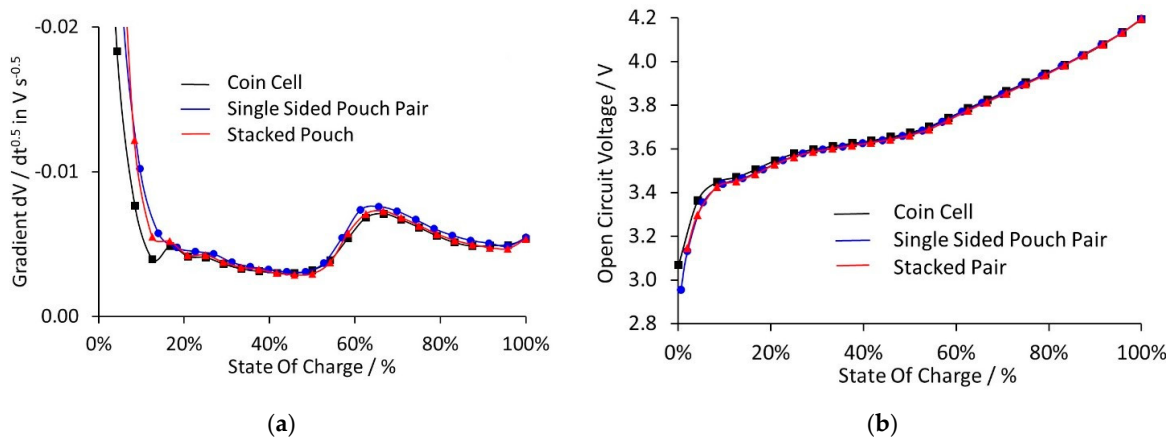


Figure 8. Parameters calculated from and measured during GITT discharge experiments, with (a) voltage gradient and (b) open circuit voltages.

It is possible to calculate values for the diffusion coefficient, as a function of state of charge (and temperature), using an equation of the form [32]:

$$D = \frac{4I^2L^2}{\Pi} \cdot \left(\frac{dE}{dQ} \right)^2 / \left(\frac{dE}{dt^{0.5}} \right)^2, t \ll L^2/D$$

The gradients $dE/dt^{0.5}$ and dE/dQ can be determined from the graphs in Figure 8, and the current I is known from the experiment. The main issue is obtaining the diffusion path length, L . The original GITT theory was developed for thin film electrodes, with linear diffusion between the surface and a blocking current collector. The electrodes used in lithium-ion cells are actually composites of millions of small particles, each with their own size, shape and orientation. Thus, it is surprising that the transients show clear linearity of voltage against time^{0.5}. Diffusion occurs within the layers of active materials like graphite and NMC. In graphite, it is neither linear nor spherical. In NMC materials, diffusion across the layers within the individual primary particles could be approximated to spherical diffusion in the secondary particles. Thus, the diffusion path length could be anywhere between the thickness of the coating and the average radius of the individual particles. An alternative approach is to estimate L from the molar volume and effective surface area [20].

3. Discussion

The differences between the three cell formats on the four main tests are summarised in Table 4. In cycling tests, the coin cells lost capacity more rapidly than the stacked pouch cells. During cycling at $\pm C/2$, the number of cycles to 80% of initial capacity was around 300 cycles for coin cells, compared to an extrapolated 1000 cycles for stacked pouch cells. For $\pm 3 C$ cycling, the equivalent number were ~1000 and ~1600 cycles. The single sided pouch pairs showed more variability, which will improve with greater optimisation of the cell format and design. The better cells gave results close to the stacked pouch cells. At present, a larger batch size is necessary to provide definitive results. In particular, the degree of compression achieved during cell manufacturing determines whether the main degradation process is thermal or mechanical.

Table 4. Summary of comparative performance of different cell formats.

Test	Coin Cells	Single Sided Pouch	Stacked Pouch
Continuous discharge	Better rate performance in anode half cells than cathode	Comparable to cathode coin cell half cells	Slightly higher areal capacities, at higher rates
Pulsed discharge	Similar gradients during diffusion-controlled stages, across all three cell formats		Higher initial voltage drop
ASI resistances	Higher in half cells, due to the lithium metal SEI layer	Slightly lower than coin cells	Not measured
GITT measurements	Consistent across all three formats, except at very low states of charge		

There are numerous possible degradation reactions that can occur in lithium-ion cells during cycling [38,39]. A common cause of resistance increase is growth of the SEI layer on the anode. This is a temperature dependent process, accelerating at higher temperatures [38]. The stacked pouch cells have a much lower mass: capacity ratio and will therefore experience higher internal temperatures, for equivalent tests. Thus, the rate of resistance increase from SEI growth should be higher in stacked pouch cells, which was observed experimentally.

Loss of active lithium is usually associated with mechanical degradation processes, from the isolation of individual particles to wholesale delamination of coatings. Lithiation and delithiation of active materials is associated with expansion and contraction of the particles. In pouch cells, this process can be measured using experiments based on Archimedes' displacement principle [40]. However, in coin cells, there is a spring applying compression

to the electrode layers. Therefore, mechanical damage and hence loss of active lithium will be more rapid in coin cells. For the single sided pouch cells, degradation reactions can be caused by mechanical or thermal factors. If the electrode pair is tightly compressed, then heat transfer will be good, but mechanical damage will be accelerated. If the electrode pair is loosely compressed, then heat transfer will be poor, but mechanical damage will be minimised. In this cell format, close attention needs to be paid to the depth of the pouch, and the thickness of the inert spacer, to achieve a consistent degree of compression.

According to the theory developed to interpret GITT experiments [30–32], if plots of voltage against time^{0.5} are linear, then the cell is expected to be under solid state diffusion control. If the voltage curves away from linearity, the implication is that a different process has become limiting, for example, saturation or depletion at the surface of the active material particles, restricted ionic conductivity, or in the worst case, lithium plating [41]. The gradients of $\Delta V / \Delta t^{0.5}$ were calculated using linear regression. The gradients were similar in all the cells, apart from one stacked pouch cell, which was in a slightly different state of charge. There was a clear difference between the charge and discharge steps, i.e., an asymmetry in the solid-state diffusion mechanism. More extreme asymmetry has been observed previously in equivalent tests on electrodes extracted from commercial lithium-ion cells [41]. The most likely cause of the asymmetry was the presence of heterogeneous layers, e.g., the diffusion coefficients of lithium in graphite and the SEI layer are different [42].

The diffusion limited reactions were common to stacked pouch cells and single sided pair pouches. However, the voltage drops depended on the actual current, and hence the cell format and capacity. The initial voltage drops were smaller with single pair pouch cells, but the stacked pouch cells gave higher discharge capacities at 30 C. This was due to a further factor, temperature. The single sided pair pouches generated a small amount of heat, even during a continuous high-rate discharge. This can be dissipated through the tabs, and the cells remained close to the set temperature. It is difficult to measure changes in external temperature using thermocouples on this cell format [43]. The stacked pouch cells generated much more heat, increasing the cell external (and internal) temperature. This can improve the reaction kinetics and increase the discharge capacity, provided that the cells did not reach a damagingly high temperature.

4. Materials and Methods

Double sided anode and cathode coatings were prepared, with relatively low coat weights. The design capacities were 1.0 mA h cm⁻² for the cathode, and 1.1 mA h cm⁻² for the anode, based on 60 gsm for the cathode, and 30 gsm for the anode. The anode was graphite based, containing Hitachi SMG-A5: CMC: SBR: C65: CNT = 91: 1.2: 1.8: 5: 1.2 wt%. The cathode was NMC-622: PVDF 5130: LITX50: KS6L = 92: 1.75: 4.25: 2 wt%. (CMC = carboxy methyl cellulose, SBR = styrene butadiene rubber, CNT = carbon nanotubes, NMC-622 = LiNi_{0.6}Mn_{0.2}Co_{0.2}O₂, and PVDF = polyvinylidene difluoride). The anode was prepared using a Bühler high speed mixer and coated on 12 µm copper foil using a Megtec reverse comma bar coater. The cathode was prepared with a Bühler high torque mixer and coated on 20 µm aluminium foil. After an initial drying stage, the electrodes were calendared down to the target porosities of 40% (anode) and 33% (cathode), using an Innovative Machine Corporation (IMC) calender. Single sided sections of the same coatings were calendared in a similar manner and used to make the coin cells and single sided pouch cells.

Stack pouch cells were assembled using production line equipment supplied by Sovema. The anode active area was 70 × 50 mm, and the cathode 68.5 × 48.5 mm. The cells contained 18 cathodes and 19 anodes, assembled using a Z fold stacking machine [44]. The end pieces were double sided anode coatings. The separator was Celgard® H1609 (Celgard LLC, Charlotte, NC, USA). The electrolyte was 1 mol dm⁻³ LiPF₆ in EC:EMC = 3:7 vol, with 1 wt% VC, from Soulbrain, MI, USA. The single sided pouch pair cells were prepared using essentially the same equipment, but they were hand wound rather than machine stacked. A 3 mm thick polyethylene spacer was used to fill out the pouch in the cell. The coin cells

were prepared using Hohsen 2032 cell components. The anodes had a diameter of 15.0 mm, and the cathodes 14.8 mm. Metal spacers (1 mm + 0.5 mm thicknesses) were used to fill out the cell volume, both placed between the negative electrode and the spring. Half cells were prepared with pre-cut disks of lithium metal, also with a diameter of 15.0 mm.

The cells were formed using a $\pm C/20$ charge and discharge cycle. The stacked pouch cells were degassed and re-sealed after this cycle. Cells from each batch were then allocated to either long term cycling or rate and performance tests. The stacked pouch cells were tested on a Maccor 4000 series cycler, with a 10 A channel limit. For higher rate pulse tests, four channels were paralleled together, to give a 40 A limit. The single sided pair cells were tested on a Maccor 4000 series cycler, with four current ranges up to 5 A. All of these tests occurred with the cells inside an environmental test chamber, set to 25 °C. Most of the coin cell tests used a Bio-Logic BCS-805 cycler, with multiple current ranges up to 150 mA. The cells were connected directly to the front of the cycler, in a room air conditioned to 25 °C. Some of the coin cell tests used the 5 A Maccor unit.

The cycling tests at $\pm C/2$ and $\pm 3 C$ used a CC-CV charge protocol, and voltage limits of 2.5 V and 4.2 V. The CV steps were stopped when the current fell to one tenth of the CC step value. The periodic cell characterisation test on the $\pm 3 C$ cycling regime involved the following steps: three cycles at $\pm C$, a full charge, a 60% discharge, a one hour rest, a ten second pulse at 5 C, and then a forty second rest. The DC resistance was calculated from $R = (V_A - V_B)/(I_A - I_B)$, where "A" is the end of the 5 C pulse, and "B" is the end of the subsequent rest. The same equation was used to calculate the ASI values. The test protocol was based on the ANL methodology [29]. Following a full charge, ten second discharge and charge pulses were performed at nine states of charge between 90% and 10%. A further charge was followed by two second pulses at 50% SoC, and thirty second pulses at 20% SoC. In each case the discharge pulse was at 1.8 C, and the charge pulse at 1.2 C. The pulse tests at different rates occurred with the cells charged to 3.65 V. A sequence of two second pulses was followed by a set of ten second pulses. Each discharge pulse was followed by a low-rate charge step, to maintain the state of charge, and vice versa.

5. Conclusions

The same anode and cathode coatings have been used to prepare lithium-ion cells in three different formats: coin cells, single sided pouch pairs, and stacked pouch cells. Stacked cells are the ultimate determinant of cell performance, but require much greater time, effort, and quantity of materials to prepare. The smaller cell sizes provide an indication of the performance in a full-sized cell, but we have shown some systematic differences between formats. Within each cell format, improvements are likely to be retained through scaled up cells.

The dominant degradation mechanism depended on the cell format. Loss of active lithium is associated with mechanical processes, e.g., compression leading to particle isolation, whereas increases in cell resistance are associated with thermally activated processes like SEI growth. Coin cells have a relatively high thermal mass but contain a relatively powerful spring. Therefore, the main degradation process was mechanical, leading to faster capacity loss but minimal resistance increase. Stacked pouch cells have a low mass: capacity ratio but can expand and contract. The main degradation process was thermal, leading to faster resistance increases, but slower capacity loss.

The conclusion from the rate, pulse and ASI tests is that the ultimate performance of stacked pouch cells is not fully reflected in tests on smaller cells. However, within each cell type, relative comparisons are useful and informative. Most of the screening and development work during the project used coin cells. However, periodically the mixing and coating was scaled up to allow stacked pouch cells to be manufactured. These cells also showed improvements, in line with those observed in the coin cell tests.

Overall, this work shows that the scale up process from coin cells to stacked pouch cells (and by implication prismatic and cylindrical cells) is not simple. It is important to understand the different contributions of mechanical and thermal factors to degradation

process in each cell format. Further work is required to predict stacked pouch cell performance from coin cell tests with greater accuracy, and to understand different contributions to degradation processes and cell resistance. However, any improvements made in one cell format can be transferred across to other cell formats and designs.

Supplementary Materials: The following are available online at <https://www.mdpi.com/article/10.3390/batteries7020038/s1>, Table S1. Calculations for Different Cell Formats and Areal Capacities Table S2. Cell Allocation for Tests after Formation Table S3. Initial Voltage Drops during Pulses At 50 % State of Charge Figure S1. Further formation cycle results with (A) cell voltages during formation cycle, (B) first cycle loss values, (C) areal discharge energies from formation cycle and (D) areal excess of anode capacity. Figure S2. Coulombic efficiency measurements during cycling at (A) $\pm C/2$ and (B) $\pm 3 C$. Figure S3. Average voltage calculations for cycling at $\pm C/2$, for (A) charge, (B) discharge, (C) shift voltage, and (D) resistance voltage. Figure S4. DC resistance measurements using 5 C pulses during cycling at $\pm 3 C$, with (A) all cells before cycling, (B) all cells after 1000 cycles, (C) a coin cell, and (D) a single sided pouch pair. Figure S5. Cell voltages during ASI measurements for (A) a higher resistance coin cell, (B) other full cells, (C) anode coin cell half cells, and (D) cathode coin cell half cells. Figure S6. Calculated ASI values for (A) full cells during charge pulses, (B) full cells during discharge pulses, (C) anode coin cell half cells, and (D) cathode coin cell half cells. Figure S7. Voltage transients during ten second pulses at 50 % state of charge, for (A) single sided pouch pair cells, (B) coin cell full cells, (C) anode coin cell half cells, and (D) cathode coin cell half cells. Figure S8. Discharge (or delithiation) voltages at different rates for (A) a single sided pouch pair cell, (B) a stacked pouch cell, (C) an anode coin cell half cell, and (D) a cathode coin cell half cell. Figure S9. Cell voltages during pulses for (A+B) single sided pouch pair cell, (C+D) stacked pouch cell, (A+C) two second pulse duration, and (B+D) ten second pulse duration. Figure S10. Cell voltages during GITT discharge pulses for (A) a coin cell, (B) a single sided pouch pair, (C) a stacked pouch cell, and (D) all cells at low states of charge.

Author Contributions: Conceptualisation, E.K. and M.C.; methodology, all; investigation, M.J.C., G.B. and J.B.; formal analysis, M.J.L.; writing—original draft preparation, M.J.L.; writing—review and editing, E.K., M.C., M.J.C., and M.J.L.; supervision, E.K. and M.C.; resources, E.K. and M.C. All authors have read and agreed to the published version of the manuscript.

Funding: WMG would like to thank the Advanced Propulsion Centre (www.apc.co.uk) for funding this project.

Institutional Review Board Statement: Not applicable.

Informed Consent Statement: Not applicable.

Data Availability Statement: Processed data is presented within the paper and supplementary information. Access to the original data is restricted by contractual requirements.

Conflicts of Interest: The authors declare no conflict of interest.

References

1. Kwade, A.; Haselrieder, W.; Leithoff, R.; Modlinger, A.; Dietrich, F.; Droeder, K. Current status and challenges for automotive battery production technologies. *Nat. Energy* **2019**, *3*, 290–300. [[CrossRef](#)]
2. Lain, M.J.; Brandon, J.; Kendrick, E. Design strategies for high power vs. high energy lithium ion cells. *Batteries* **2019**, *5*, 64. [[CrossRef](#)]
3. Karulkar, M.; Wren, H.; Kudla, B.; Blaser, R. Evaluation of silicon based cells and the importance of scale up. *ECS Trans.* **2016**, *72*, 197–206. [[CrossRef](#)]
4. Scheifele, W.; Joho, F.; Rykart, B.; Novák, P. Scale up of lithium ion batteries: From a coin cells to a 12 A h battery. *PSI Sci. Rep.* **1999**, *5*, 64–65.
5. Majima, M.; Ujiie, S.; Yagasaki, E.; Koyama, K.; Inazawa, S. Development of long life lithium ion battery for power storage. *J. Power Sources* **2001**, *101*, 53–59. [[CrossRef](#)]
6. Mangang, M.; Seifert, H.J.; Pfleging, W. Influence of laser pulse duration on the electrochemical performance of laser structured LFP composite electrodes. *J. Power Sources* **2016**, *304*, 24–32. [[CrossRef](#)]
7. Trask, S.E.; Li, Y.; Kubal, J.J.; Bettge, M.; Polzin, B.J.; Zhu, Y.; Jansen, A.N.; Abraham, D.P. From coin cells to 400 mA h pouch cells: Enhancing performance of high capacity lithium ion cells via modifications in electrode construction and fabrication. *J. Power Sources* **2014**, *359*, 233–244. [[CrossRef](#)]

8. Chen, S.; Niu, C.; Lee, H.; Li, Q.; Yu, L.; Xu, W.; Zhang, J.-G.; Dufek, E.J.; Whittingham, M.S.; Meng, S.; et al. Critical parameters for evaluating coin cells and pouch cells of rechargeable lithium metal batteries. *Joule* **2019**, *4*, 1095–1105. [[CrossRef](#)]
9. Cheng, X.-B.; Yan, C.; Huang, J.-Q.; Li, P.; Zhu, L.; Zhao, L.; Zhang, Y.; Zhu, W.; Yang, S.T.; Zhang, Q. The gap between long lifespan Li-S coin and pouch cells: The importance of lithium metal anode protection. *Energy Storage Mater.* **2017**, *6*, 18–25. [[CrossRef](#)]
10. Bauer, W.; Nötzel, D.; Wenzel, V.; Nirsch, H. Influence of dry mixing and distribution of conductive additives in cathodes for lithium ion batteries. *J. Power Sources* **2015**, *288*, 359–367. [[CrossRef](#)]
11. INL/EXT-14-32849. USABC Battery Test Manual for PHEV; Idaho National Laboratory: Idaho Falls, ID, USA, 2010. [[CrossRef](#)]
12. An, S.J.; Li, J.; Mohanty, D.; Daniel, C.; Polzin, B.J.; Croy, J.R.; Trask, S.E.; Wood III, D.L. Correlation of electrolyte volume and electrochemical performance in lithium ion pouch cells with graphite anodes and NMC532 cathodes. *J. Electrochem. Soc.* **2017**, *164*, A1195–A1202. [[CrossRef](#)]
13. Yourey, W. Theoretical impact of manufacturing tolerances on lithium ion electrode and cell physical properties. *Batteries* **2020**, *6*, 23. [[CrossRef](#)]
14. Müller, V.; Scurtu, R.-G.; Richter, K.; Waldmann, T.; Memm, M.; Danzer, M.A.; Wohlfahrt-Mehrens, M. Effect of mechanical compression on the ageing and expansion behaviour of Si/C composite / NMC811 in different lithium ion cell battery cell formats. *J. Electrochem. Soc.* **2019**, *166*, A3796–A3805. [[CrossRef](#)]
15. Abraham, D.P.; Knuth, J.L.; Dees, D.W.; Bloom, I.; Christophersen, J.P. Performance degradation of high power lithium ion cells—Electrochemistry of harvested electrodes. *J. Power Sources* **2007**, *170*, 465–475. [[CrossRef](#)]
16. Zhang, Q.; White, R.E. Calendar life study of lithium ion pouch cells. *J. Power Sources* **2007**, *173*, 990–997. [[CrossRef](#)]
17. Watanabe, S.; Kinoshita, M.; Nakura, K. Capacity fade of NCA cathode for lithium ion batteries during accelerated calendar and cycle life tests. I. Comparison analysis between NCA and LCO cathodes in cylindrical lithium ion cells during long term storage test. *J. Power Sources* **2014**, *247*, 412–422. [[CrossRef](#)]
18. Schmid, A.U.; Kurka, M.; Birke, K.P. Reproducibility of lithium ion cell reassembling processes and their influence on coin cell ageing. *J. Energy Storag.* **2019**, *24*, 100732. [[CrossRef](#)]
19. Schindler, S.; Danzer, M.A. Influence of cell design on impedance characteristics of cylindrical lithium ion cells: A model based assessment from electrode to cell level. *J. Energy Storag.* **2017**, *12*, 157–166. [[CrossRef](#)]
20. Chen, C.-H.; Planella, F.B.; O'Regan, K.; Gastol, D.; Widanage, W.D.; Kendrick, E. Development of experimental techniques for parameterisation of multi scale lithium ion battery models. *J. Electrochem. Soc.* **2020**, *167*, 080534. [[CrossRef](#)]
21. Quinn, J.B.; Waldmann, T.; Richter, K.; Kasper, M.; Wohlfahrt-Mehrens, M. Energy density of cylindrical lithium in cells: A comparison of commercial 18650 to 21700 cells. *J. Electrochem. Soc.* **2018**, *165*, A3284–A3291. [[CrossRef](#)]
22. Waldmann, T.; Scurtu, R.-G.; Richter, K.; Wohlfahrt-Mehrens, M. 18650 vs. 21700 lithium ion cells—A direct comparison of electrochemical, thermal and geometric properties. *J. Power Sources* **2020**, *472*, 228614. [[CrossRef](#)]
23. Kim, H.-K.; Choi, J.H.; Lee, K.-J. A numerical study of the effects of cell formats on the cycle life of lithium ion batteries. *J. Electrochem. Soc.* **2019**, *166*, A1769–A1778. [[CrossRef](#)]
24. Rheinfeld, A.; Sturm, J.; Frank, A.; Kosch, S.; Erhard, S.V.; Jossen, A. Impact of cell size and format on external short circuit behaviour of lithium ion cells at varying cooling conditions: Modelling and simulation. *J. Electrochem. Soc.* **2020**, *167*, 013511. [[CrossRef](#)]
25. Murray, V.; Hall, D.S.; Dahn, J.R. A guide to full coin cell making for academic researchers. *J. Electrochem. Soc.* **2019**, *166*, A329–A333. [[CrossRef](#)]
26. Long, B.R.; Rinaldo, S.G.; Gallagher, K.G.; Dees, D.W.; Trask, S.E.; Polzin, B.J.; Jansen, A.N.; Abraham, D.P.; Bloom, I.; Barenco, J.; et al. Enabling high energy, high voltage lithium ion cells: Standardisation of coin cell assembly, electrochemical testing and evaluation of full cells. *J. Electrochem. Soc.* **2016**, *163*, A2999–A3009. [[CrossRef](#)]
27. Okasinski, J.S.; Shkrob, I.A.; Chuang, A.; Fonseca Rodrigues, M.-T.; Raj, A.; Dees, D.W.; Abraham, D.P. In Situ x-ray spatial profiling reveals uneven compression of electrode assemblies and steep lateral gradients in lithium ion coin cells. *Phys. Chem. Chem. Phys.* **2020**, *22*, 21977–21986. [[CrossRef](#)] [[PubMed](#)]
28. Bockwinkel, K.; Nowak, C.; Thiede, B.; Nöske, M.; Dietrich, F.; Thiede, S.; Haselrieder, W.; Dröder, K.; Kwade, A.; Hermann, C. Enhanced processing and testing concepts for new active materials for lithium ion batteries. *Energy Technol.* **2020**, *8*, 1900133. [[CrossRef](#)]
29. Lu, W.; Jansen, A.; Dees, D.; Nelson, P.; Veselka, N.R.; Henriksen, G. High energy electrode investigation for PHEV. *J. Power Sources* **2011**, *196*, 1537–1540. [[CrossRef](#)]
30. Weppner, W.; Huggins, R.A. Electrochemical methods for determining kinetic properties of solids. *Ann. Rev. Mater. Sci.* **1978**, *8*, 269–311. [[CrossRef](#)]
31. Wen, C.J.; Boukamp, B.A.; Huggins, R.A.; Weppner, W. Thermodynamic and mass transport properties of LiAl. *J. Electrochem. Soc.* **1979**, *126*, 2258–2266. [[CrossRef](#)]
32. Markevich, E.; Levi, M.D.; Aurbach, D. Comparison between potentiostatic and galvanostatic intermittent titration techniques for determination of chemical diffusion coefficients in ion insertion electrodes. *J. Electroanal. Chem.* **2005**, *580*, 231–237. [[CrossRef](#)]
33. Harlow, J.E.; Glazier, S.L.; Li, J.; Dahn, J.R. Use of asymmetric average charge and average discharge voltages as an indicator of the onset of unwanted lithium deposition in lithium ion cells. *J. Electrochem. Soc.* **2018**, *165*, A3595–A3601. [[CrossRef](#)]

34. Holsttiege, F.; Wilken, A.; Winter, M.; Placke, T. Running out of lithium? A route to differentiate between capacity losses and active lithium losses in lithium ion batteries. *Phys. Chem. Chem. Phys.* **2017**, *19*, 25905–25918. [[CrossRef](#)] [[PubMed](#)]
35. Nelson, P.A.; Gallagher, K.G.; Bloom, I.; Dees, D.W. *Modelling the Performance and Cost of Lithium-Ion Batteries for Electric-Drive Vehicles*; Argonne National Lab: Argonne, IL, USA, 2012. [[CrossRef](#)]
36. Gallagher, K.G.; Nelson, P.A.; Dees, D.W. Simplified calculation of the area specific impedance for battery design. *J. Power Sources* **2011**, *196*, 2289–2297. [[CrossRef](#)]
37. Ragone, D. Review of battery systems for electrically powered vehicles. *SAE Tech. Paper* **1968**, 680453. [[CrossRef](#)]
38. Barré, A.; Deguilhem, B.; Grolleau, S.; Gérard, M.; Suard, F.; Riu, D. A review of lithium ion battery ageing mechanisms and estimations for automotive applications. *J. Power Sources* **2013**, *241*, 680–689. [[CrossRef](#)]
39. Birk, C.R.; Roberts, M.R.; McTurk, E.; Bruce, P.G.; Howey, D.A. Degradation diagnostics for lithium ion cells. *J. Power Sources* **2017**, *341*, 373–386. [[CrossRef](#)]
40. Aiken, C.P.; Xia, J.; Wang, D.Y.; Stevens, D.A.; Trussler, S.; Dahn, J.R. An apparatus for the study of in situ gas evolution in lithium ion pouch cells. *J. Electrochem. Soc.* **2014**, *161*, A1548–A1554. [[CrossRef](#)]
41. Lain, M.J.; Kendrick, E. Understanding the limitations of lithium ion batteries at high rates. *J. Power Sources* **2021**, *493*, 229690. [[CrossRef](#)]
42. Alvarez-Ramirez, J.; Dagdug, L.; Meraz, M. Asymmetric diffusion in heterogeneous media. *Physica A* **2014**, *395*, 193–199. [[CrossRef](#)]
43. Heubner, C.; Schneider, M.; Lämmel, C.; Michaelis, A. Local heat generation in a single stack lithium ion battery cell. *Electrochim. Acta* **2015**, *186*, 404–412. [[CrossRef](#)]
44. Kurfer, J.; Westermeier, M.; Tammer, C.T.; Reinhart, G. Production of larger area lithium ion cells—Pre-conditioning, cell stacking and quality assurance. *CIRP Ann.* **2012**, *61*, 1–4. [[CrossRef](#)]